Halftoning by Rotating Non-Bayer Dispersed Dither Arrays *

Victor Ostromoukhov, Roger D. Hersch
Ecole Polytechnique Fédérale de Lausanne (EPFL)
CH-1015 Lausanne, Switzerland
victor@di.epfl.ch, hersch@di.epfl.ch

Abstract

We propose a new operator for creating rotated dither threshold arrays. This new discrete one-to-one rotation operator is briefly explained. We analyze its application to different dispersed-dot dither arrays such as hexagonal dispersed dither arrays and 3x3 matrix-based Bayer-expanded dither arrays and compare the results with the ones obtained by rotating standard Bayer dither arrays. We show that the rotation operator introduces new lower-frequency components which, for example in the case of rotated dispersed-dot Bayer dither, produces a slight clustering effect improving the tone reproduction behavior of the halftone patterns. In other cases, such as hexagonal dispersed dither, these new lower frequency components are responsible for strong interferences in the rotated halftone array. When applied to 3x3 matrix-based Bayer-expanded dither arrays, the rotation operator induces sequences of short horizontal and vertical patterns, which have a very good tone reproduction behavior in the dark tones. Besides their use in black and white printing, rotated dispersed-dot dither halftoning techniques have also been successfully applied to in-phase color reproduction on ink-jet printers.

Keywords

Printing, halftoning, dispersed-dot dithering, Bayer dither, 3x3 matrix-based Bayer-expanded dither, hexagonal dither, discrete one-to-one rotation, dot gain, reproduction behavior, spatial-frequency analysis.

1 Introduction

In a recent contribution published in the SIGGRAPH'94 Conference Proceedings [Ostromoukhov94], the authors proposed a new dithering technique for digital halftoning: rotated dispersed-dot dither. It was introduced for the discrete one-to-one rotation of Bayer dispersed-dot dither arrays. Discrete rotation has the effect of rotating and splitting the frequency impulses present in non-rotated halftone arrays onto a new spatial frequency grid, thereby producing many new low-frequency impulses which, for certain types of halftone arrays such as Bayer's, have a low amplitude.

Rotating the original halftone patterns provides a way to avoid the horizontal and vertical components present in most of Bayer's halftone patterns. The resulting frequency components, which have diagonal orientations, are less disturbing to the eye than horizontal and vertical patterns found in Bayer's halftones. Furthermore, since

[1] IS&T/SPIE 1995 International Symposium on Electronic Imaging: Science & Technology, February 4 – 10, 1995, San Jose, California, Proceedings Conf. Human Vision, Visual Processing and Digital Display VI, SPIE Vol. 2411.

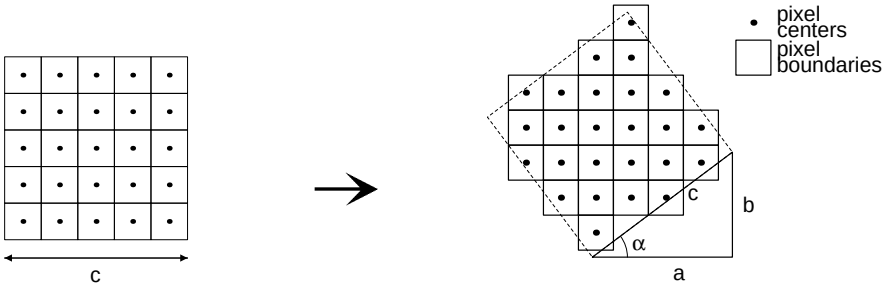

Figure 1: Rotating a square array of c^2 pixels by a Pythagorean angle $\alpha = \arctan(\frac{b}{a})$, where $c = 5, a = 4$, $b = 3$.

the discrete rotation operator creates a new spatial-frequency grid with a lower basic frequency, discrete rotation has a clustering behavior which leads to an improved gray tone reproduction behavior for printers having a non-negligible dot gain.

After briefly showing previous results obtained with rotated Bayer dispersed-dot dither matrices (section 2), this paper explores the effect of discrete one-to-one rotation applied to dispersed dither matrices whose dispersion patterns differ from Bayer's. In section 3, we consider hexagonally dispersed-dot matrices similar to those proposed by Ulichney [Ulichney87]. These hexagonally dispersed dither matrices are produced by repeatedly applying a tile expansion algorithm with self-similarity factor 3 to a an initial 3-element hexagonal array. We show that the discrete rotation applied to the 3 sets of frequencies present in the considered hexagonal halftone array induces a strong interference pattern.

In section 4, we consider the rotation of a non-Bayer well-dispersed dither array produced by applying Bayer's dither expansion rule to a 3x3 well-dispersed original dither matrix. While the non-rotated halftone patterns have similar horizontal and vertical components as Bayer's, their rotated counterparts behave nicely, i.e they include small sequences of connected horizontal and vertical components which improve their tone reproduction behavior.

In section 5, we plot the tone reproduction curves associated with the presented dispersed-dot halftoning methods and discuss their respective advantages and disadvantages.

2 The rotated dither method applied to Bayer's dispersed-dot dither halftones

Bayer's dispersed-dot ordered dither method has been shown to be optimal in the sense that in each gray level, the lowest frequency is as high as possible [Bayer73]. Nevertheless, as Fig. 20c shows, low frequency components given by the dither array period size are quite strong for a large number of gray levels. These low frequency halftoning artifacts are well perceived, since at increasing intensity levels they switch back and forth from horizontal and vertical to diagonal directions. The transition between one intensity level and the next one creates an abrupt pattern change which appears in the halftoned image as a false contour (Fig. 20c).

Since human eye sensitivity to gratings decreases considerably at oblique orientations [Campbell66], we can make the perceived halftoning artifacts less visible by rotating the dispersed dither array. Moreover, the examples shown in section 5 raise the assumption that discrete rotation of the dispersed dither array decreases the power of the individual low-frequency components by distributing their low-frequency energy over a larger set of frequencies.

The discrete rotation we apply to dither arrays has some similarities with the rotation of bitmap images. For the sake of simplicity, we will therefore also use in this context the term "pixel" to denote a simple dither array element. The rotating task consists of finding a discrete rotation, which generates a "rotated Bayer threshold array" whose threshold values are exactly the values of the original Bayer dither threshold array. Let us consider

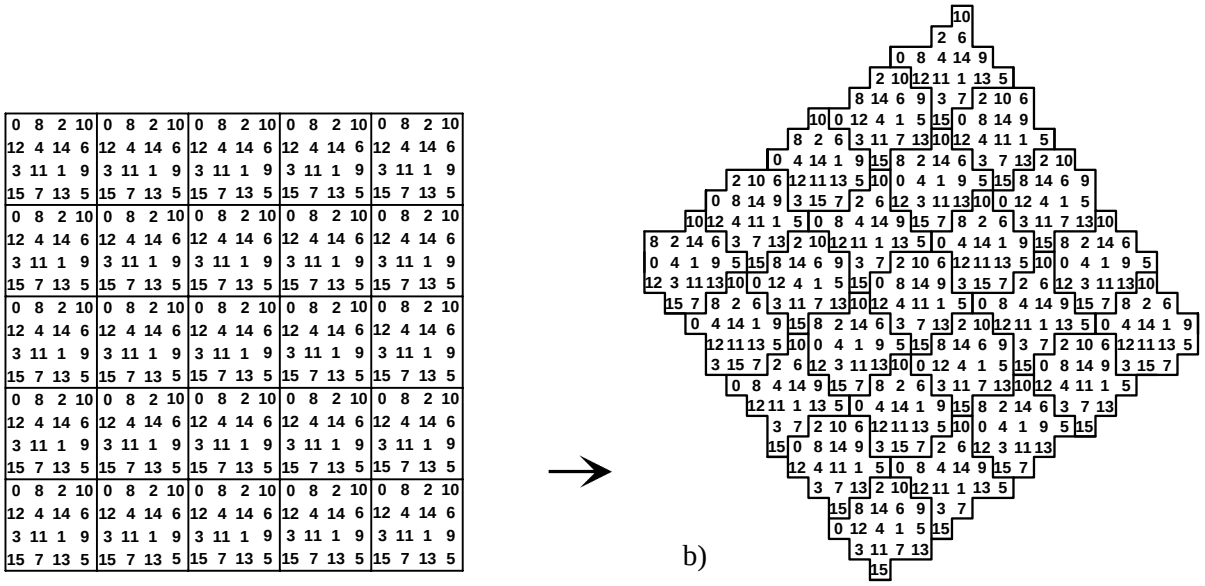

Figure 2: (a) Original replicated dither threshold array D^{c*n} and (b) rotated dither tile R^{c*n} obtained by the discrete rotation of tile D^{c*n}.

rotations of binary pixel grids composed of unit size pixel squares. Exact rotation of a square pixel grid by an angle α around the position (x_0, y_0) can be described by the following transformation applied to the pixel centers (x, y):

$$\begin{aligned} x' &= (x - x_0)\cos\alpha - (y - y_0)\sin\alpha + x_0 \\ y' &= (x - x_0)\sin\alpha + (y - y_0)\cos\alpha + y_0 \end{aligned} \tag{1}$$

In the general case, more than one rotated original pixel center may fall within a single pixel square boundary in the destination grid, and some destination pixels may remain empty [Hersch85]. We therefore need a one-to-one discrete rotation which unambiguously maps the set of original dither array elements into the new set formed by the rotated dither array.

Let us consider the continuous boundary of a square array of c^2 discrete pixels (Figure 1). It can be shown that if this boundary is rotated by a Pythagorean angle $\alpha = \arctan(b/a)$, where a and b are Pythagorean numbers satisfying the Diophantine equation $a^2 + b^2 = c^2$, the resulting rotated square boundary contains the same number of pixel centers as the original pixel array (Figure 1). Therefore, a discrete one-to-one rotation can be obtained by rotating with a Pythagorean angle and by an appropriate one-to-one mapping between the set of dither elements belonging to the original square and the set of dither elements belonging to the rotated square.

Such a discrete one-to-one rotation is obtained by rotating with a Pythagorean angle $\alpha = \arctan(b/a)$, where $c = 5$, $a = 4$, $b = 3$ and $\alpha = \arctan(3/4) = 36.87^\circ$ and by applying rounding operations. Let us assume that (i, j) is the coordinate system of the original dither array and (x, y) the coordinate system of the rotated dither array, and that i_0, j_0, and respectively x_0, y_0 are integer values defining the location of the given original square dither array, respectively the location of the rotated dither array:

$$\begin{aligned} x &= \text{round}\left(\frac{a}{c} * (i - i_0) - \frac{b}{c} * (j - j_0)\right) + x_0 \\ y &= \text{round}\left(\frac{b}{c} * (i - i_0) + \frac{a}{c} * (j - j_0)\right) + y_0 \end{aligned} \tag{2}$$

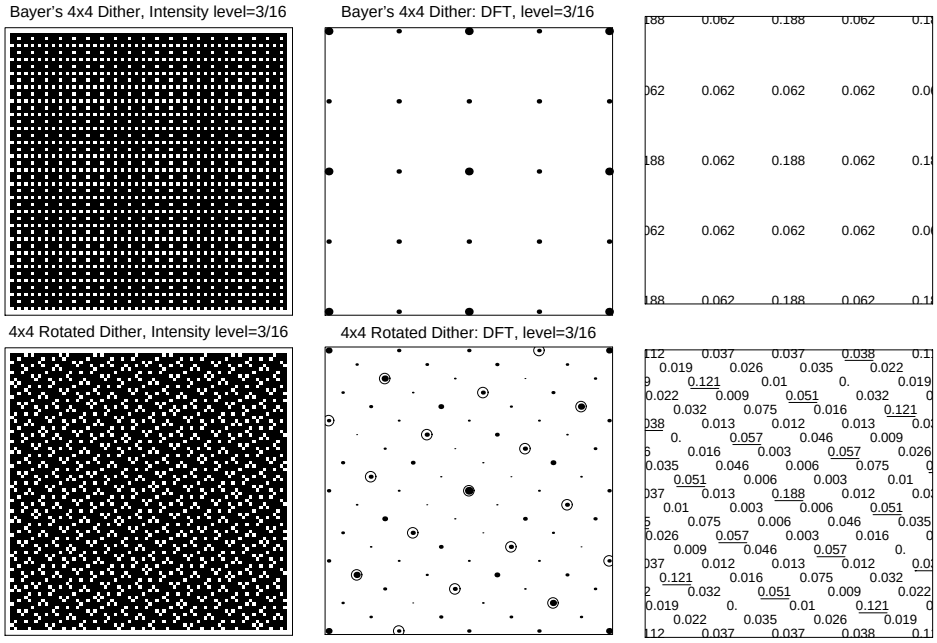

Figure 3: Halftone patterns at grayscale level $\frac{3}{16}$, created according to Bayer's 4x4 dispersed-dot dither array (above) and according to the rotated dither method (below), as well as their corresponding Fourier amplitude spectra.

In order to apply this discrete one-to-one rotation to a square Bayer dither threshold array, we have to consider the Bayer threshold array D^n of size nxn, replicated c times vertically and horizontally, since its side length must be an integer multiple of Pythagorean hypotenuse c (Figure 2a). We will denote the dither tile obtained this way by D^{c*n}. In Figure 2 we use the Bayer dither threshold array of size $n = 4$.

The discrete one-to-one rotation described by equations 2 applied to a dither tile D^{c*n} made of a replicated Bayer dither threshold array yields a rotated dither tile R^{c*n} (Figure 2b), which also paves the plane like the original tile D^{c*n}. The elements of the rotated dither tile R^{c*n} have the same dither values as the corresponding original dither elements from the dither tile D^{c*n}.

As can be seen from Figure 20e, rotated dispersed-dot halftoning generates less texture artifacts than the standard Bayer method. Moreover, as can be seen in the gray wedges at the top of the images, the tone reproduction of rotated dither is much better than that of the Bayer dither.

In order to compare the proposed rotated dither algorithm with Bayer's dispersed-dot dither algorithm, we analyze their respective halftone patterns at various intensity levels by comparing their frequency amplitude spectra. It is well known that the human eye is most sensitive to the lowest frequency components of screen dot patterns, especially if they have a horizontal or vertical orientation. Bayer demonstrated that his ordered dither algorithm minimizes the occurrence of low-frequency components. However, he didn't take into account the amplitudes of the spectral frequencies, nor did he consider the anisotropic behavior [Campbell66] of the eye's contrast sensitivity function (CSF).

To compare the two dither algorithms, we consider a halftone pattern, representing gray level $\frac{3}{16}$. In that example, the Holladay rectangle paving the corresponding rotated dither tile has a size of 20 by 4 pixels [Holladay80]. By choosing a sample array of a size which is an integer multiple of the horizontal and vertical replication period of the dither rectangle paving the plane, we ensure that the frequencies present in the Discrete

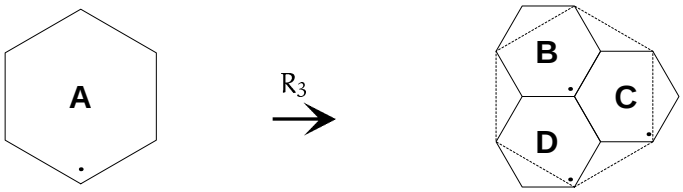

Figure 4: Decomposition of a hexagonal screen element A into three similar hexagonal screen elements B, C and D, according to an inflation rule R_3.

Fourier Transform (DFT) of the sample array are located exactly on the spatial-frequency sampling grid, thereby avoiding leakage effects and ensuring that the spectral impulses fall exactly on the center of DFT impulses [Brigham88].

In the examples shown in Figure 3, we consider 80x80 pixel sample halftone arrays created according to Bayer's 4x4 dispersed-dot dither array and according to the rotated dither method, using 4x4 dispersed-dot dither arrays, replicated 5 times and rotated. Figure 3 shows the halftone patterns as well as their corresponding DFT impulse amplitudes at grayscale level $\frac{3}{16}$. The dot surfaces in the spectra are proportional to the amplitude of the corresponding frequency impulses.

The following observations can be made:

Compared to Bayer's dither, rotated dither frequency impulses lie on a new, lower frequency oblique quadratic grid. The grid is formed by the multiples of the original discretely rotated frequency components folded back into the discrete base frequency band limited by the sampling rate (for more details, see section 3). The discrete rotation reduces the energy of the original frequency impulses and distributes the energy difference throughout the new denser spatial-frequency grid. The fundamental frequency of the new lower frequency grid determines the aliasing pattern observable in the amplitude spectrum. Its amplitude gives the strength of the corresponding aliasing effect (see Fig 3).

We can therefore conclude that the rotated dither method rotates the frequency impulses present in the Bayer halftone array and splits one part of their amplitude into lower frequency impulses. The power of the original Bayer main frequency components is therefore reduced, and additional low frequency components are created. When these new low frequency components are weak, as is the case of the rotated Bayer dither, the corresponding low-frequency patterns do not induce visually disturbing artifacts. Moreover, since the main frequency components are rotated, they are less perceptible to the human eye than the horizontal and vertical components present in most of Bayer's halftone patterns.

3 Creating and rotating hexagonally dispersed-dot dither arrays

This section section begins by describing a recursive algorithm for the generation of hexagonal dither arrays on a hexagonal pixel grid. A simple modification is all that is required to adapt these dither arrays to quadratic pixel grids. We then evaluate the quality of the resulting dispersed hexagonal dither patterns. Finally, we show why, in this case, the discrete one-to-one rotation generates unacceptable aliasing effects.

Screen elements of hexagonal shape, i.e. screen elements which each have six direct neighbors can easily be built when the rendering device has a regular hexagonal or nearly-hexagonal pixel grid. Regular nearly-hexagonal grids are available on visualization devices, where the centers of output samples (or pixels) in every second scanline have a horizontal offset of half the horizontal sampling period. Methods already exist for synthesizing hexagonal screen elements having appropriate angles and periods in their 3 main directions [Ulichney87].

Nevertheless, for the sake of clarity, we will describe here our own method for creating hexagonal dispersed-dot dither tiles of various sizes.

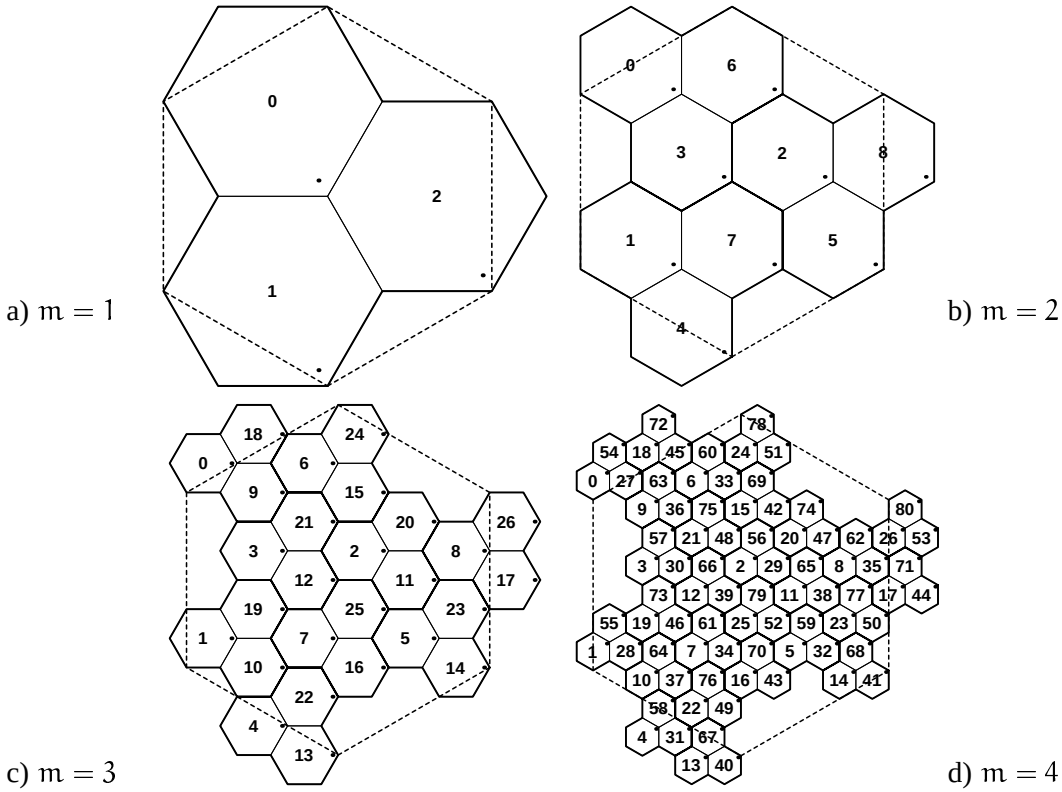

Figure 5: Regular hexagonal tiles subdivided into $3, 9, 27$ and 81 smaller hexagonal sub-tiles after respectively $m = 1, 2, 3$ and 4 inflations R_3.

Let A be a hexagonal screen element, as shown in Figure 4. It can be decomposed into three similar hexagonal screen elements B, C and D, according to an inflation rule R_3 (Figure 4b). Both original tile A and decomposed tile BCD pave the plane.

The decomposition process according to the inflation rule R_3 can be continued iteratively, as shown in Figure 5. Starting from a regular hexagonal shape (dashed line in Figure 5), the tile contains $3, 9, 27$ and 81 smaller hexagonal sub-tiles after respectively $m = 1, 2, 3$ and 4 inflations (see Figure 5). All these tiles pave the plane. Consequently, any of them can be considered to be the *fundamental tile* of a regular tiling [Grunbaum89].

Let us adopt the following numbering convention:

$$\begin{cases} V_B^{(m+1)} = V_A^{(m)} \\ V_C^{(m+1)} = V_A^{(m)} + 3^m \\ V_D^{(m+1)} = V_A^{(m)} + 2 * 3^m \end{cases} \tag{3}$$

where $V_A^{(m)}$, respectively $V_B^{(m+1)}$, $V_C^{(m+1)}$ are numbers associated with elements A before, respectively B, C and D after the m-th inflation according to inflation rule R_3. Figure 5 shows the fundamental tile obtained after $m = 1, 2, 3$ and 4 inflations, with numbers affected according to numbering convention (3).

The numbers in the fundamental tile can be interpreted as threshold values, in the case of a hexagonal or nearly-hexagonal pixel grid. In such a case, the tile shown in Figure 5d can be used as a hexagonal well-dispersed dither matrix which provides $3^4 + 1 = 82$ different graylevels.

In the case of a quadratic pixel grid, one can build a dither matrix which is based on the hexagonal dispersion obtained according to inflation rule R_3, as described above. Figure 6 illustrates such a construction. In this figure,

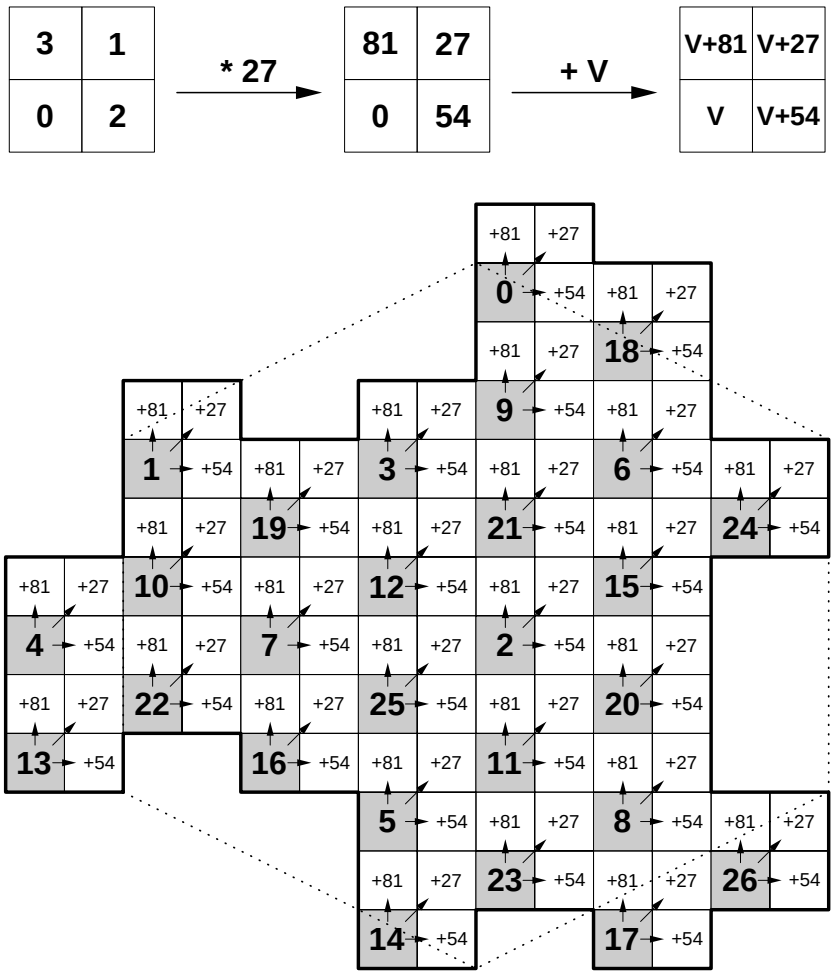

Figure 6: Construction of a dither matrix which is based on the hexagonal dispersion obtained according to inflation rule R_3, in the case of a quadratic pixel grid.

the dispersion of Figure 5c ($m = 3$, $3^3 = 27$ elementary cells) is used. We group 2x2 pixels of the quadratic grid into one cell of the hexagonal dither tile (see Figure 6), and number them according to following rules:

- the displacement vector between two 2x2 pixel groups is two pixels horizontally and one pixel vertically,

- the lower-left pixel in any 2x2 pixel group takes a value in the range $[0 - 26]$, according to the hexagonal distribution of Figure 5c, as shown in Figure 6,

- the upper-right pixel in any 2x2 pixel group takes a value in the range $[27 - 53]$, which is equal to the value of the lower-left pixel plus 27. Similarly, the value of the lower-right pixel pixel equals that of the lower-left pixel plus 54, and the value of the upper-left pixel equals that of the down-left pixel plus 81 (see Figure 6).

In this way, a dither matrix containing $4 * 3^3 = 108$ different numbers in the range $[0 - 107]$ can be constructed. Figure 7 shows the minimal square area, repetitive in both horizontal and vertical directions, which contains several nearly-hexagonal dither matrices described above, side-by-side. Obviously, such a square area contains redundant part. Nevertheless, this representation is useful when studying the Fourier spectrum of the generated halftone patterns.

Beside Figure 7, there is a representation of the sum of all amplitude spectra of the so generated halftones.

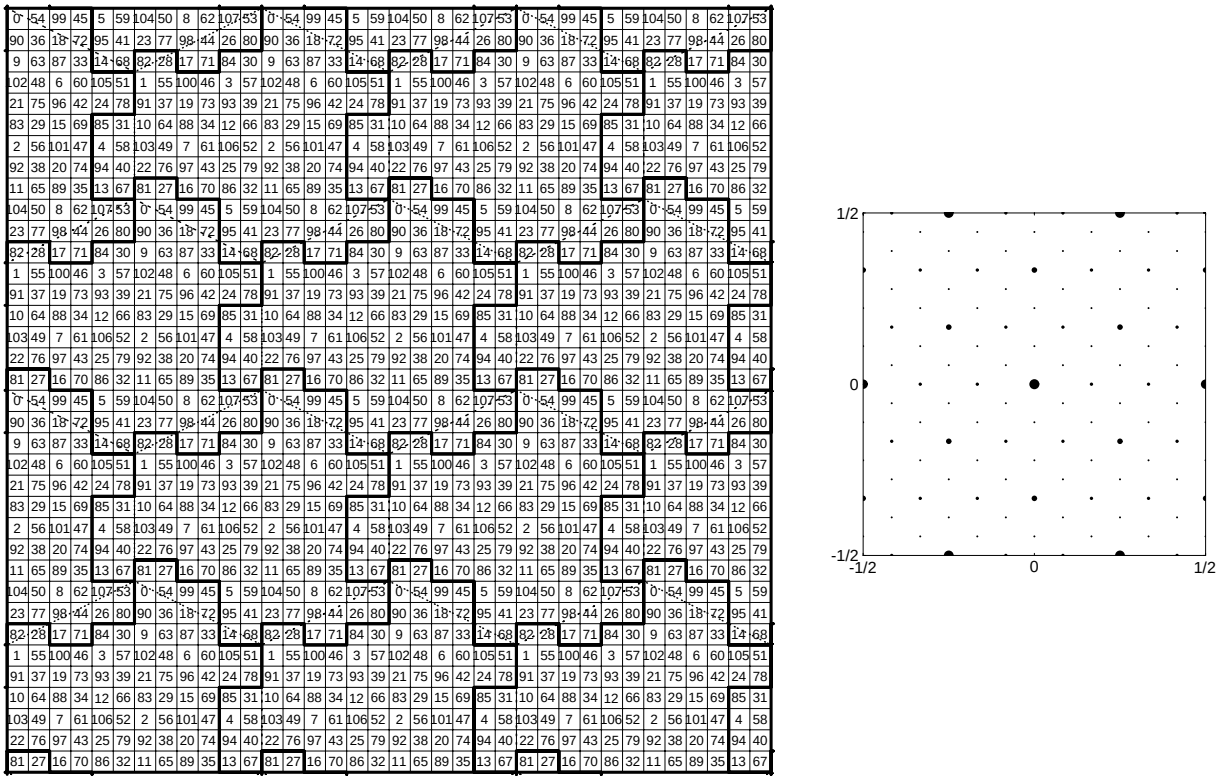

Figure 7: The minimal square area, repetitive in both horizontal and vertical directions, which contains several nearly-hexagonal dither matrices obtained according to inflation rule R_3, in the case of a quadratic pixel grid.

This representation gives precise information about the spatial frequency grid and gives global information about the relative amplitude of the different frequency impulses.

Figure 8 shows a tile paving the plane composed of a 5x5 array of hexagonal dither tiles rotated by angle $\alpha = \mathrm{arctg}(4/3)$. Each of the rotated hexagonal dither tiles is slightly different from the others (boundaries). Nevertheless, each one includes exactly the same number of cells as the original non-rotated hexagonal dither tile.

Fig. 11 shows a few halftone patterns produced by the rotated hexagonal dither array. A specially strong interference appears at intensity level 27/108. This low-frequency interference corresponds to the lowest frequency components in the amplitude spectrum (Fig. 12). Let us assume that the hexagonal halftone pattern is composed by the multiplication of 3 mono-directional signals, having each one a different orientation (see Fig 10, intensity level $\frac{27}{128}$). In this context, a mono-directional signal is defined as a two-dimensional signal varying only in one dimension. In the spectral domain, the interference is produced by the convolution of the first harmonics of 2 of the 3 signals composing the rotated hexagonal pattern. Rotated frequency impulses (1) and (2) are folded back into the original spectrum (see Fig. 13b), generating interference signal $(1') * *(2')$. Such an interference pattern does not appear in the non-rotated halftone, since the convolution of frequency impulses (1) and (2) generates impulses which, when folded back in the baseband, fall on locations determined by frequency impulses (3) (Fig. 13a).

We conclude, looking at Fig. 20d, that non-rotated hexagonal dispersed-dot dither shows a slight improvement compared with standard Bayer dispersed-dot dithering due to the fact that the horizontal and vertical components present in Bayer's dither are replaced by hexagonal elements. Nevertheless, contouring effects are similar in both cases (see for example Lenna's face, Fig. 20d). In this hexagonal dispersion case, the discrete rotation operator

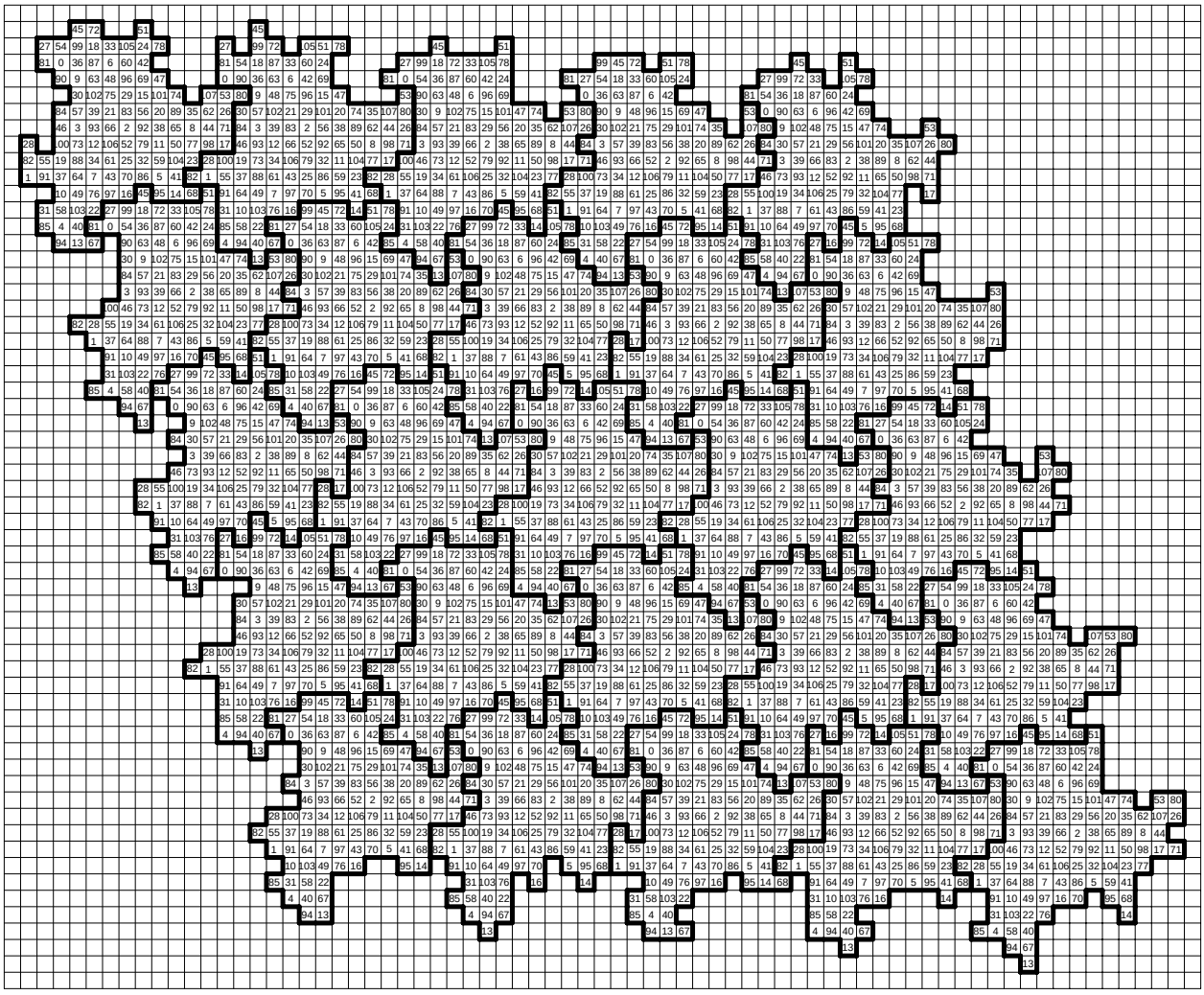

Figure 8: Fundamental tile paving the plane composed of a 5x5 array of hexagonal dither tiles rotated by angle $\alpha = \mathrm{arctg}4/3$.

fails to bring any improvement to hexagonal dispersed-dot dither due to the strong low-frequency interference it produces.

4 Rotating 3x3 matrix-based bayer-expanded dither arrays

One further method of generating dispersed-dot dither arrays consists of first generating manually a 3x3 matrix-based dispersed-dot dither array where direct neighbors have larger dither threshold differences than indirect neighbors. This 3x3 matrix-based dispersed-dot dither array is then expanded using Bayer's expansion rule, which consists of scaling the array values by a factor of 4 and replicating the scaled array 4 times. Intermediate threshold values are then added to the threshold values of the replicated scaled dither array, according to the cell locations within the new array (Fig. 14). In the spectral domain, the configuration of the halftone patterns' frequency components is quite close to Bayer's. Due to the discrete one-to-one rotation, the small, repetitive, original halftone patterns (Fig. 16) transform themselves into more complex patterns, made up of sequences of small horizontal and vertical segments (Fig. 18). A statistic comparison shows that the rotated patterns have at

least 1.5 times more direct neighbors than the non-rotated patterns. Therefore, its exhibits a stronger clustering behavior than the non-rotated halftone pattern. When analyzing the amplitude spectrum, one sees clearly lower frequency components in the rotated patterns which, however, are sufficiently weak to avoid producing a significant visual impact. The rotational operator decreases the power of the original patterns significantly (Fig. 19, halftone level 12/36). For example, the repetitive structure of the non-rotated halftone at level 12/36 (Fig. 16, can no longer be detected anymore in the rotated pattern (Fig. 18).

The rotated 3x3 matrix-based Bayer-expanded dither is a valid alternative to the rotated Bayer dispersed-dot dither matrix. It produces halftone patterns which exhibit very smooth transitions between successive grayscale levels. The small clusters made of short sequences of vertical and horizontal segments predominate at intensity levels between 1/4 to 3/4 and may be filtered out by the human visual system. Furthermore, the tone reproduction behavior at dark tones is the best with the exception of clustered-dot halftoning (Fig. 20).

5 Comparing the tone reproduction behavior of the different dispersed-dither methods

The tone reproduction behavior of a given halftoning algorithm is heavily dependent on the dot gain behavior of the considered printer. At levels darker than 50%, classical dispersed-dot dither algorithms such as Bayer's tend to generate one pixel black/one pixel white chessboards-like patterns whose white areas may shrink considerably due to dot gain. The clustering behavior of the different rotated dispersed-dot dither algorithms at mid-tones has a positive impact on their tone reproduction capabilities.

Let us compare the tone reproduction behavior of the different rotated dispersed-dot dither algorithm with Bayer's dispersed-dot dither algorithm and clustered-dot halftoning. For this purpose we measure and plot the tone reproduction behavior of a variable intensity grayscale wedge printed on a black and white laser printer. Figure 21 shows the tone reproduction behavior for the considered halftoning techniques.

If we compare the different rotated dither methods with Bayer's dither and hexagonal dither, Figure 21 clearly shows that, for printers with a certain dot gain, the two rotated dispersed-dot dither methods have a behavior closer to clustered-dot dither, especially at mid-tones. They are therefore good candidates for dispersed-dot printing on laser or on ink-jet printers (300–800 dpi) having a significant dot gain.

The rotated 3x3 matrix-based Bayer-expanded dither method has a slight advantage over the rotated Bayer dither due to its improved reproduction behavior at dark tones.

While the clustered-dot dither method is the most robust in terms of reproduction behavior at large dot gains, both the rotated Bayer and the rotated 3x3 matrix-based Bayer-expanded dispersed-dot dither methods offer a favorable reproduction behavior and good detail rendition capabilities.

6 Conclusion

We have introduced a new operator for creating rotated dither arrays. We have analyzed its application to different non-Bayer dispersed-dither arrays such as hexagonal dispersed dither arrays and 3x3 matrix-based Bayer-expanded dither arrays and compared the results with the ones obtained by rotating standard Bayer dither arrays. We show that the rotation operator induces new lower-frequency components which, both in the case of Bayer dispersed-dot dither and of 3x3 matrix-based Bayer-expanded dither, produces a slight clustering effect improving the tone reproduction behavior of the halftone patterns. In other cases, such as hexagonal dispersed dither, the new lower frequency components generated by discrete one-to-one rotation are responsible for a strong interference in the rotated halftone array.

Discrete rotation attenuates the visible frequency components belonging to the original halftone arrays by spreading part of their energy into lower frequency components. In the cases where these lower frequency components are weak, the resulting artifacts are less disturbing than the ones produced by the non-rotated dither array.

When rendering images at smoothly increasing intensity levels, the proposed rotated dispersed-dot dither methods (rotated Bayer dither and rotated 3x3 matrix-based Bayer-expanded dither) generate less contouring effects than Bayer's dither method and less artifacts than Floyd-Steinberg's error-diffusion method. Besides their use in black and white printing, rotated dispersed-dot dither halftoning techniques have also be successfully applied to in-phase color reproduction on ink-jet printers. Rotated dither halftoning techniques can also be applied to increase the number of perceived colors on display devices with a limited number of intensity levels.

Acknowledgments

We would like to thank the Swiss National Fund (grant No. 2100-040541.94/1) for supporting the project.

References

[Brigham88] E.O. Brigham, *The Fast Fourier Transform and its Applications.* Prentice-Hall, UK, 1988.

[Bayer73] B.E. Bayer, An Optimum Method for Two-Level Rendition of Continuous-Tone Pictures, *IEEE 1973 International Conference on Communications,* Vol. 1, June 1973, 26-11–26-15.

[Campbell66] F.W. Campbell, J.J. Kulikowski, J. Levinson, The effect of orientation on the visual resolution of gratings, *J. Physiology*, London, 1966, Vol 187, 427-436.

[Grunbaum89] B. Grunbaum, G.C. Shephard, *Tilings and Patterns*, W.H. Freeman and Co. N.-Y., 1989.

[Hersch85] R.D. Hersch, Raster Rotation of Bilevel Bitmap Images, *Eurographics'85 Proceedings,* (Ed. C. Vandoni), North-Holland, 1985, 295-308.

[Holladay80] Holladay T. M., "An Optimum Algorithm for Halftone Generation for Displays and Hard Copies," *Proceedings of the Society for Information Display*, 21(2), 1980, 185-192.

[Ostromoukhov94] V. Ostromoukhov, R.D. Hersch, I. Amidror, "Rotated Dispersed Dither: a New Technique for Digital Halftoning", Proceedings of SIGGRAPH'94, *ACM Computer Graphics*, Annual Conference Series, pp. 123–130, 1994.

[Ulichney87] R. Ulichney, *Digital Halftoning,* The MIT Press, Cambridge, Mass., 1987.

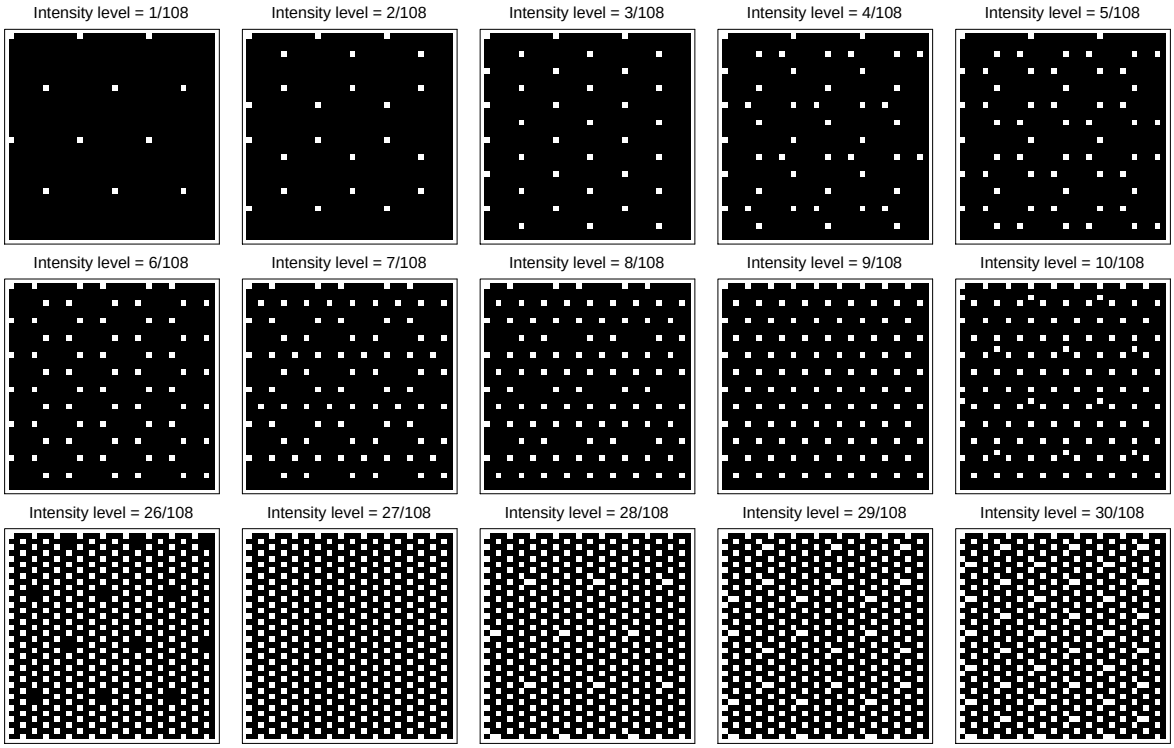

Figure 9: Halftone patterns produced by the hexagonal dither array, at several intensity levels.

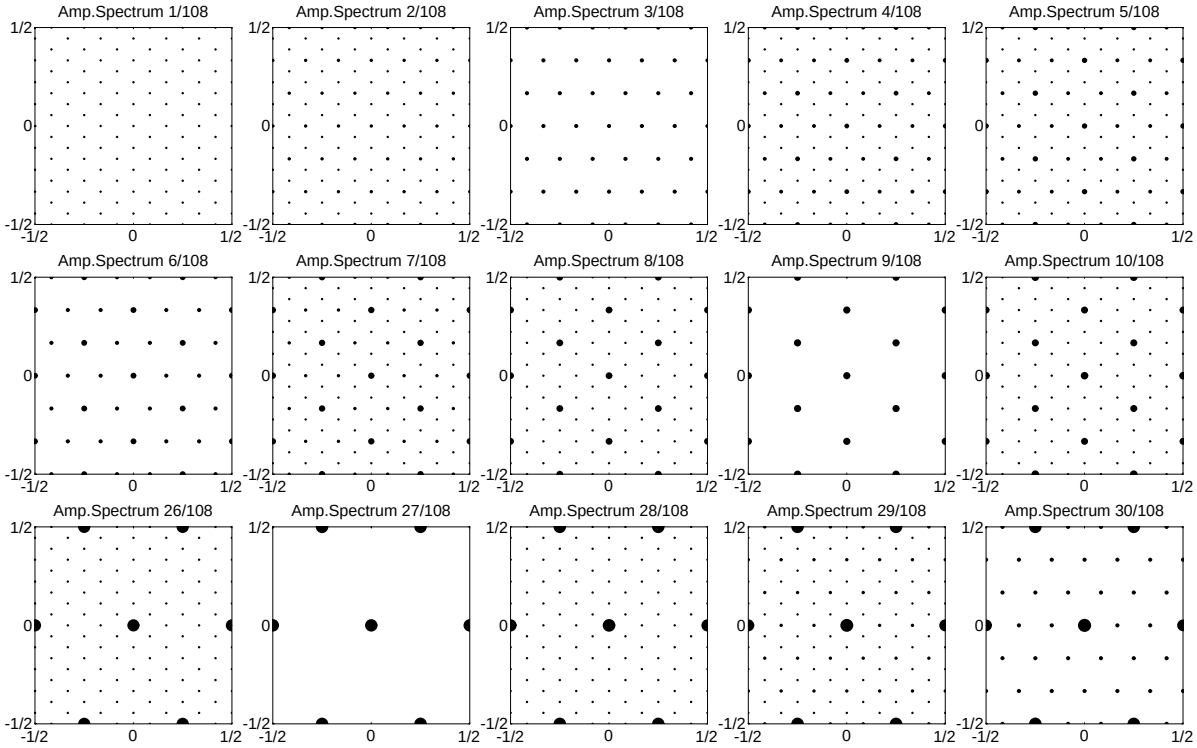

Figure 10: Amplitude spectra of the halftone patterns produced by the hexagonal dither array, at the same intensity levels.

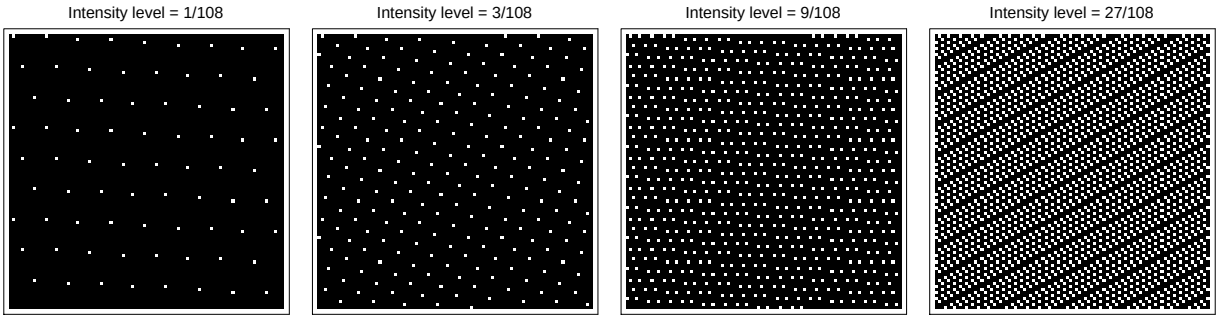

Figure 11: Halftone patterns produced by the rotated hexagonal dither array, at intensity levels $1/108, 3/108, 9/108$ and $27/108$.

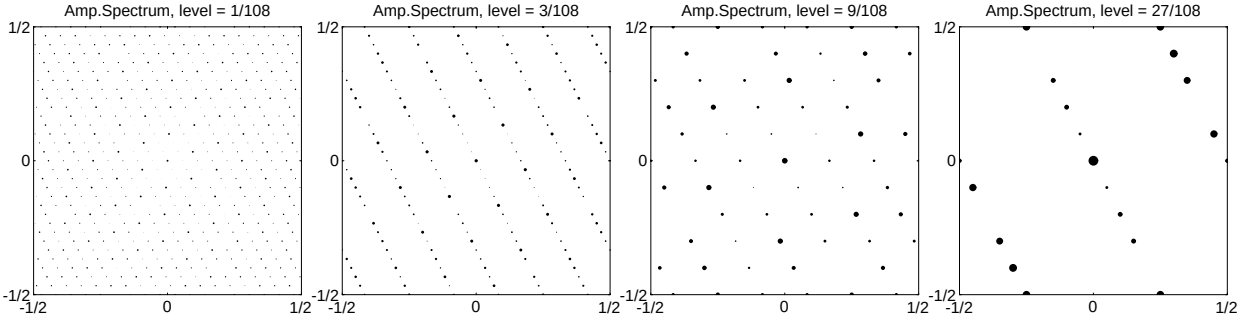

Figure 12: Amplitude spectra of the halftone patterns produced by the rotated hexagonal dither array, at intensity levels $1/108, 3/108, 9/108$ and $27/108$.

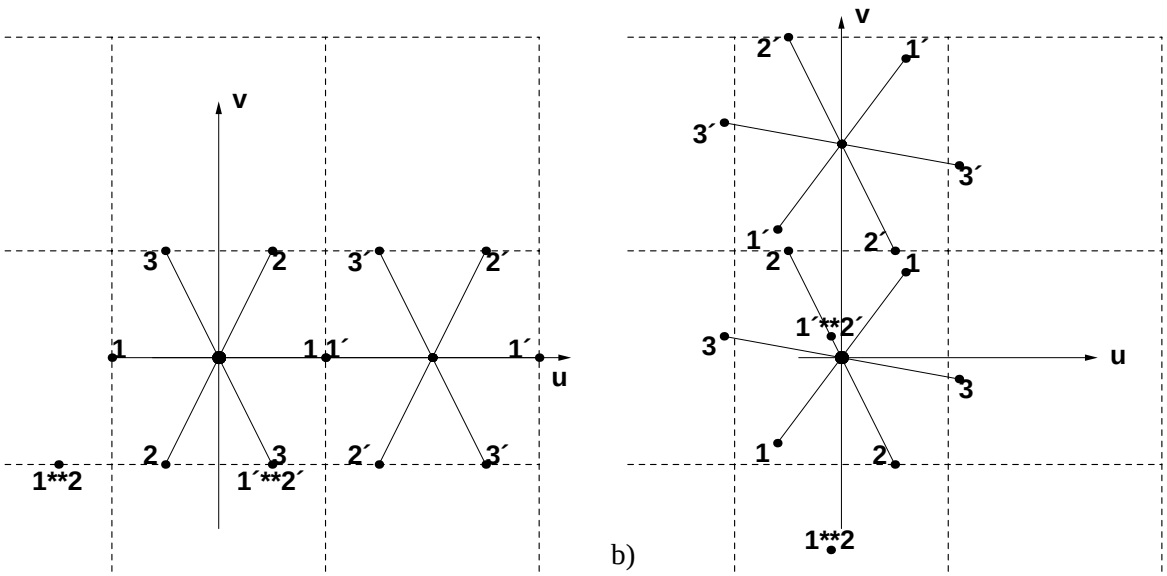

Figure 13: Partial view of the convolution of frequency components (1) and (2), folded back into the baseband limited by the sampling frequency, (a) in the case of the non-rotated hexagonal pattern and (b) in the case of the hexagonal pattern, rotated by angle $\alpha = \mathrm{arctg}(4/3)$.

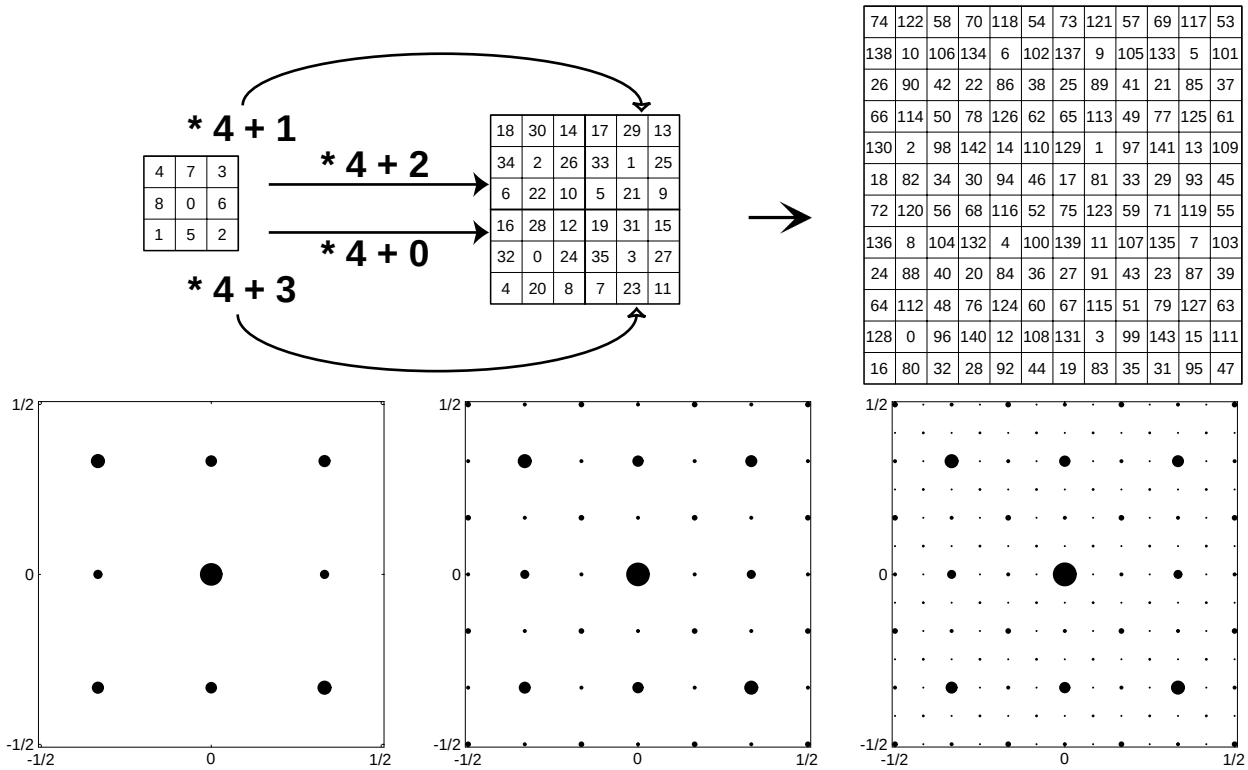

Figure 14: Construction of 3x3 matrix-based dispersed-dot dither array (a) of size 3x3, (b) of size 6x6 and (c) of size 12x12.

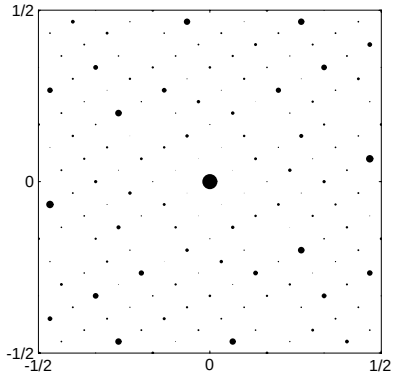

35	7	23	29	25	6	16	28	0	8	17	33	1	21	15	32	4	20	30	26	5	19	31	3	11	18	34	2	22	12
24	8	17	1	21	9	15	32	20	30	14	26	5	31	3	27	11	18	2	22	10	12	35	23	29	13	25	6	28	0
20	14	26	33	5	31	27	11	4	18	2	10	12	19	35	23	13	25	34	6	28	24	8	7	17	1	9	15	16	32
18	30	2	10	19	35	3	23	13	34	6	22	28	24	7	17	29	1	9	16	32	0	20	14	33	5	21	31	27	4
13	34	22	28	12	24	7	29	1	25	9	16	0	20	8	14	33	21	31	15	27	4	30	2	26	10	19	3	23	11
25	9	6	16	0	8	14	17	33	21	15	27	32	4	30	26	10	5	19	3	11	13	18	34	22	12	24	35	7	29
1	21	15	32	4	20	30	26	5	19	31	3	11	18	34	2	22	12	35	7	23	29	25	6	16	28	0	8	17	33
5	31	3	27	11	18	2	22	10	12	35	23	29	13	25	6	28	0	24	8	17	1	21	9	15	32	20	30	14	26
12	19	35	23	13	25	34	6	28	24	8	7	17	1	9	15	16	32	20	14	26	33	5	31	27	11	4	18	2	10
28	24	7	17	29	1	9	16	32	0	20	14	33	5	21	31	27	4	18	30	2	10	19	35	3	23	13	34	6	22
0	20	8	14	33	21	31	15	27	4	30	2	26	10	19	3	23	11	13	34	22	28	12	24	7	29	1	25	9	16
32	4	30	26	10	5	19	3	11	13	18	34	22	12	24	35	7	29	25	9	6	16	0	8	14	17	33	21	15	27
11	18	34	2	22	12	35	7	23	29	25	6	16	28	0	8	17	33	1	21	15	32	4	20	30	26	5	19	31	3
29	13	25	6	28	0	24	8	17	1	21	9	15	32	20	30	14	26	5	31	3	27	11	18	2	22	10	12	35	23
17	1	9	15	16	32	20	14	26	33	5	31	27	11	4	18	2	10	12	19	35	23	13	25	34	6	28	24	8	7
33	5	21	31	27	4	18	30	2	10	19	35	3	23	13	34	6	22	28	24	7	17	29	1	9	16	32	0	20	14
26	10	19	3	23	11	13	34	22	28	12	24	7	29	1	25	9	16	0	20	8	14	33	21	31	15	27	4	30	2
22	12	24	35	7	29	25	9	6	16	0	8	14	17	33	21	15	27	32	4	30	26	10	5	19	3	11	13	18	34
16	28	0	8	17	33	1	21	15	32	4	20	30	26	5	19	31	3	11	18	34	2	22	12	35	7	23	29	25	6
15	32	20	30	14	26	5	31	3	27	11	18	2	22	10	12	35	23	29	13	25	6	28	0	24	8	17	1	21	9
27	11	4	18	2	10	12	19	35	23	13	25	34	6	28	24	8	7	17	1	9	15	16	32	20	14	26	33	5	31
3	23	13	34	6	22	28	24	7	17	29	1	9	16	32	0	20	14	33	5	21	31	27	4	18	30	2	10	19	35
7	29	1	25	9	16	0	20	8	14	33	21	31	15	27	4	30	2	26	10	19	3	23	11	13	34	22	28	12	24
14	17	33	21	15	27	32	4	30	26	10	5	19	3	11	13	18	34	22	12	24	35	7	29	25	9	6	16	0	8
30	26	5	19	31	3	11	18	34	2	22	12	35	7	23	29	25	6	16	28	0	8	17	33	1	21	15	32	4	20
2	22	10	12	35	23	29	13	25	6	28	0	24	8	17	1	21	9	15	32	20	30	14	26	5	31	3	27	11	18
34	6	28	24	8	7	17	1	9	15	16	32	20	14	26	33	5	31	27	11	4	18	2	10	12	19	35	23	13	25
9	16	32	0	20	14	33	5	21	31	27	4	18	30	2	10	19	35	3	23	13	34	6	22	28	24	7	17	29	1
31	15	27	4	30	2	26	10	19	3	23	11	13	34	22	28	12	24	7	29	1	25	9	16	0	20	8	14	33	21
19	3	11	13	18	34	22	12	24	35	7	29	25	9	6	16	0	8	14	17	33	21	15	27	32	4	30	26	10	5

Figure 15: 3x3 matrix-based dispersed-dot dither array of size 6x6, after discrete 1-to-1 rotation by angle $\alpha = \mathrm{arctg}(4/3)$.

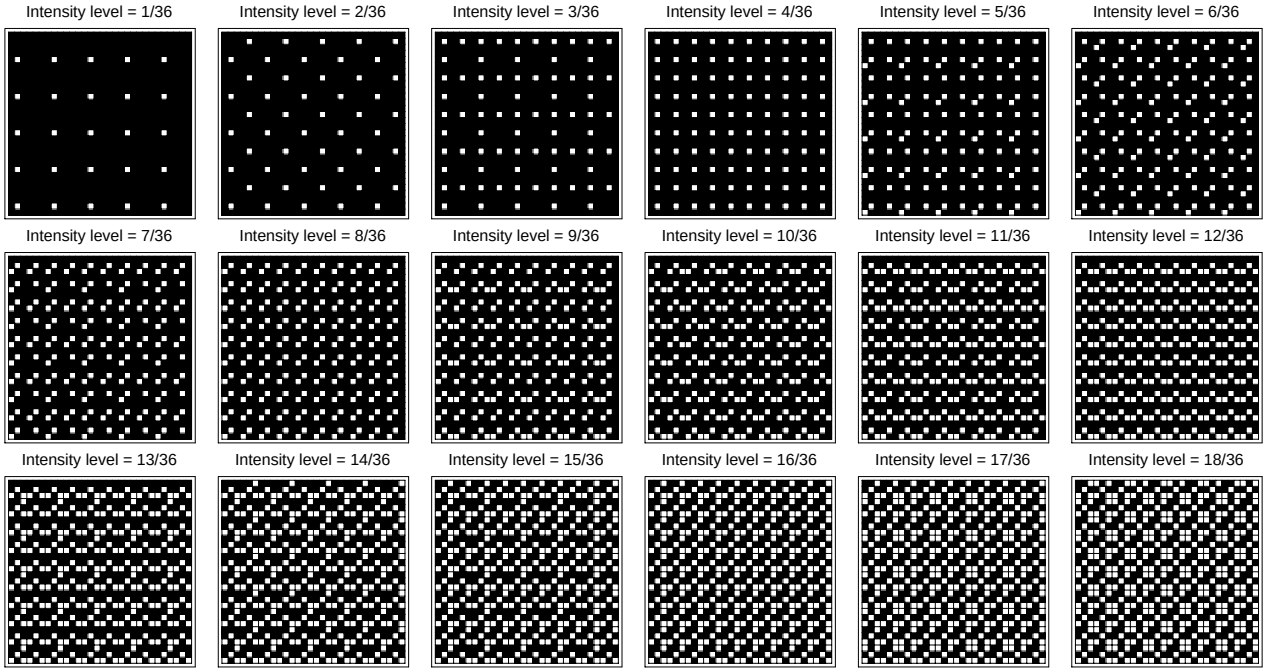

Figure 16: Halftone patterns produced by the 3x3 matrix-based dispersed-dot dither array, at several intensity levels.

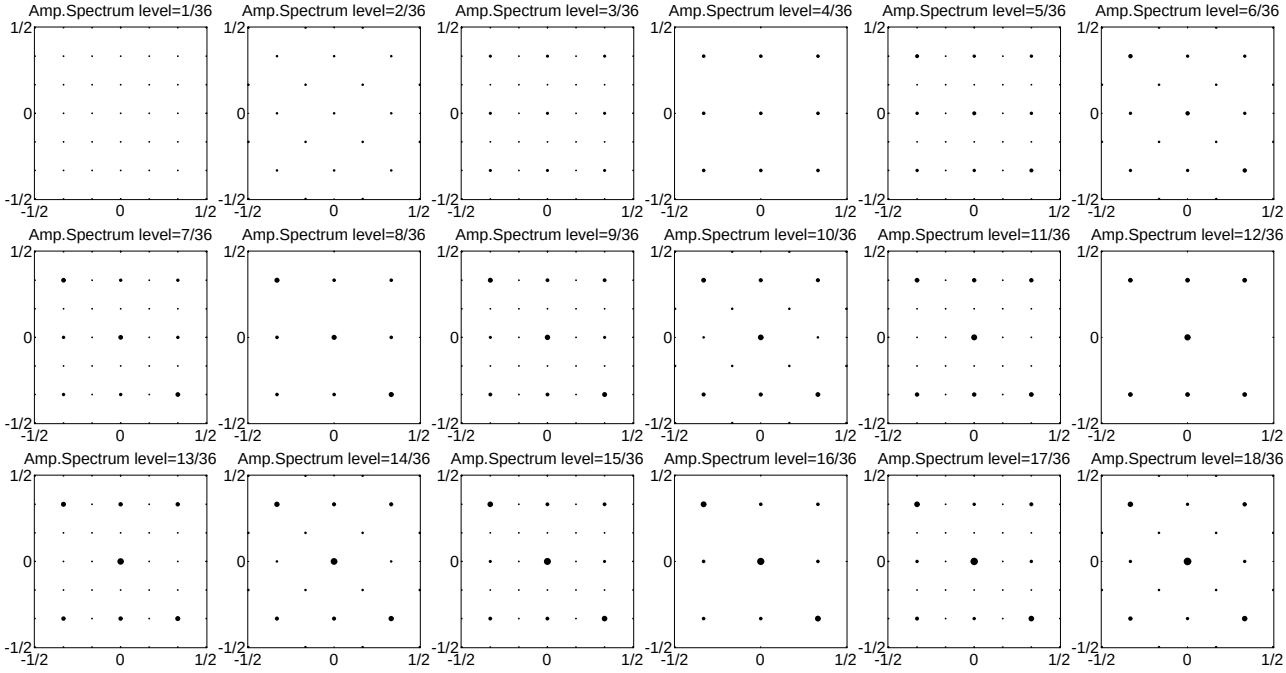

Figure 17: Amplitude spectra of the halftone patterns produced by the 3x3 matrix-based dispersed-dot dither array, at the same intensity levels.

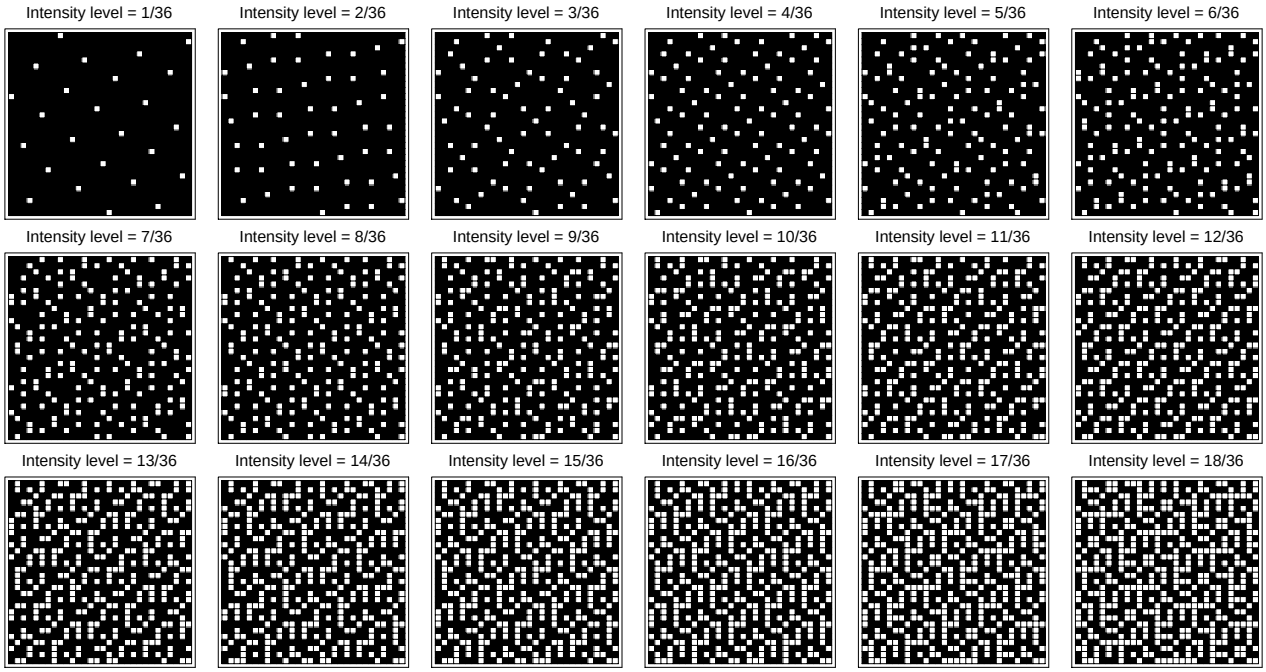

Figure 18: Halftone patterns produced by the rotated 3x3 matrix-based dispersed-dot dither array, at several intensity levels.

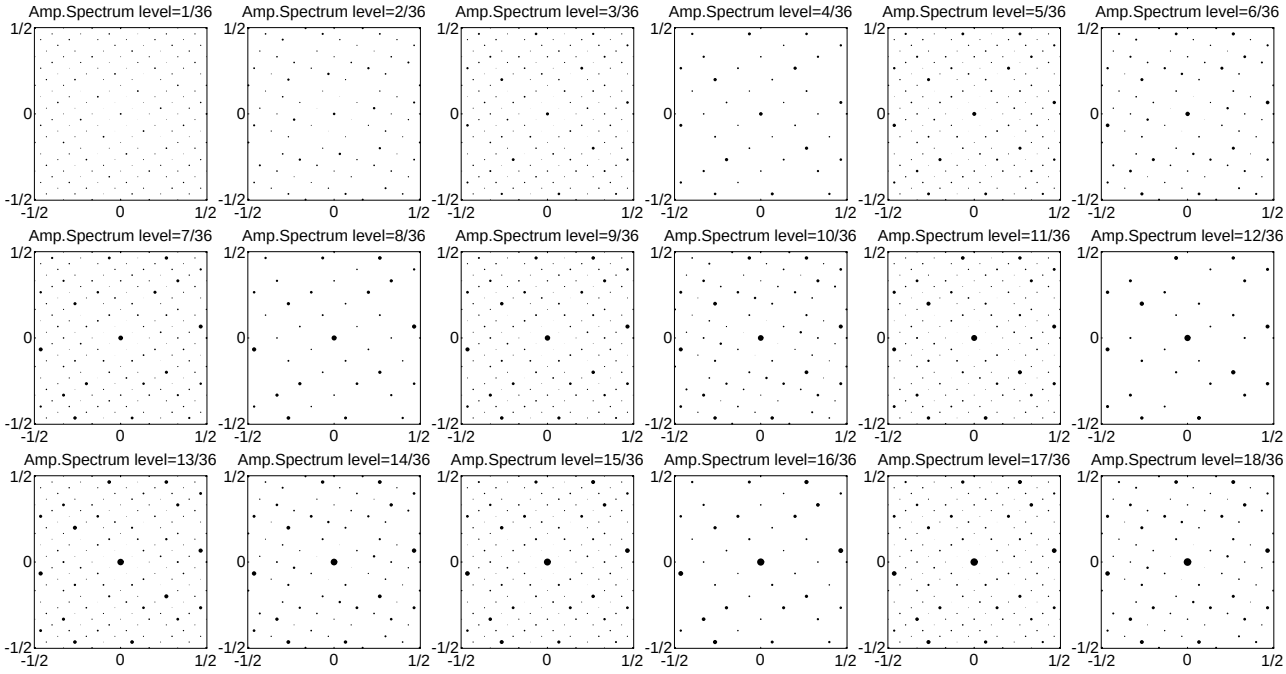

Figure 19: Amplitude spectra of the halftone patterns produced by the rotated 3x3 matrix-based dispersed-dot dither array, at the same intensity levels.

Figure 20: Grayscale image, halftoned at 300 dpi with (a) a conventional diagonally oriented clustered-dot dither array, (b) error diffusion. (c) 16x16 Bayer's dither algorithm, (d) hexagonal dispersed-dot dither, (e) rotated Bayer's dispersed-dot dither (f) rotated 3x3 matrix-based Bayer-expanded dither. Gamma correction applied.

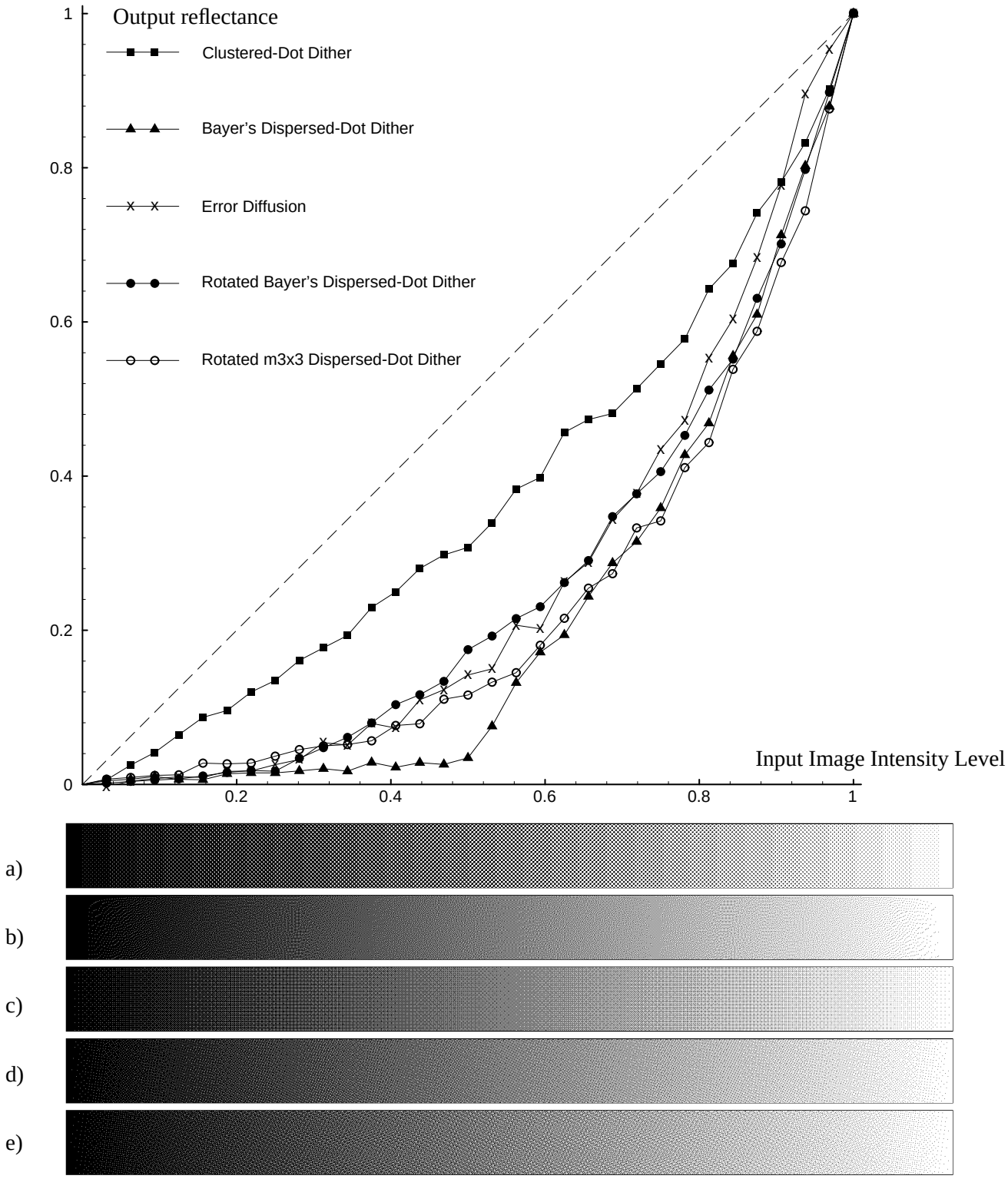

Figure 21: Tone reproduction curves obtained from density measurements of wedges printed at 300 dpi on a laser printer. (a) a conventional diagonally oriented clustered-dot dither array, (b) error diffusion. (c) 16x16 Bayer's dither algorithm, (d) rotated Bayer's dispersed-dot dither (e) rotated 3x3 matrix-based Bayer-expanded dither.

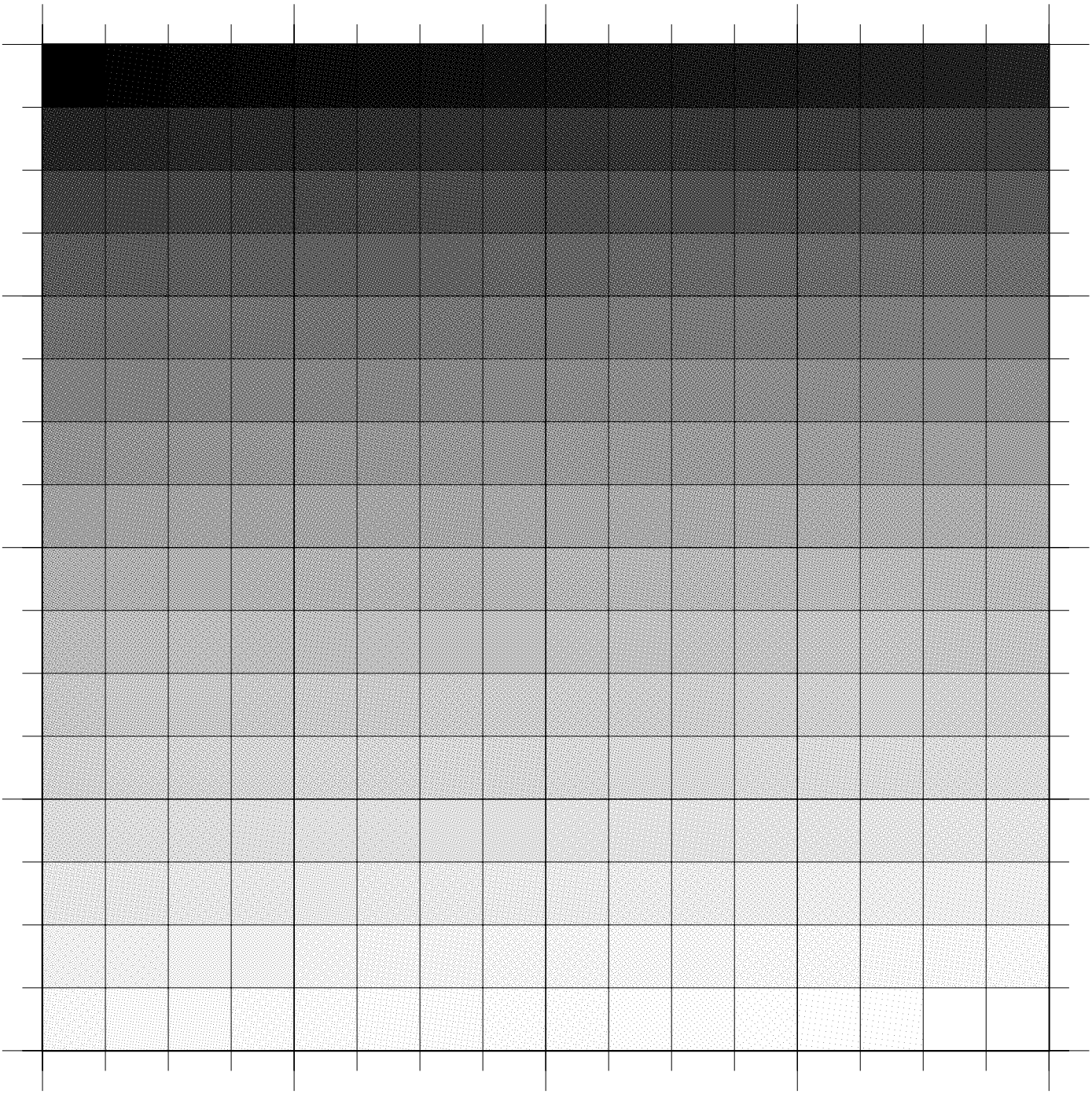

Figure 22: 256 intensity levels obtained with rotated Bayer's dispersed-dot dither algorithm, printed at 300 dpi on a laser printer.

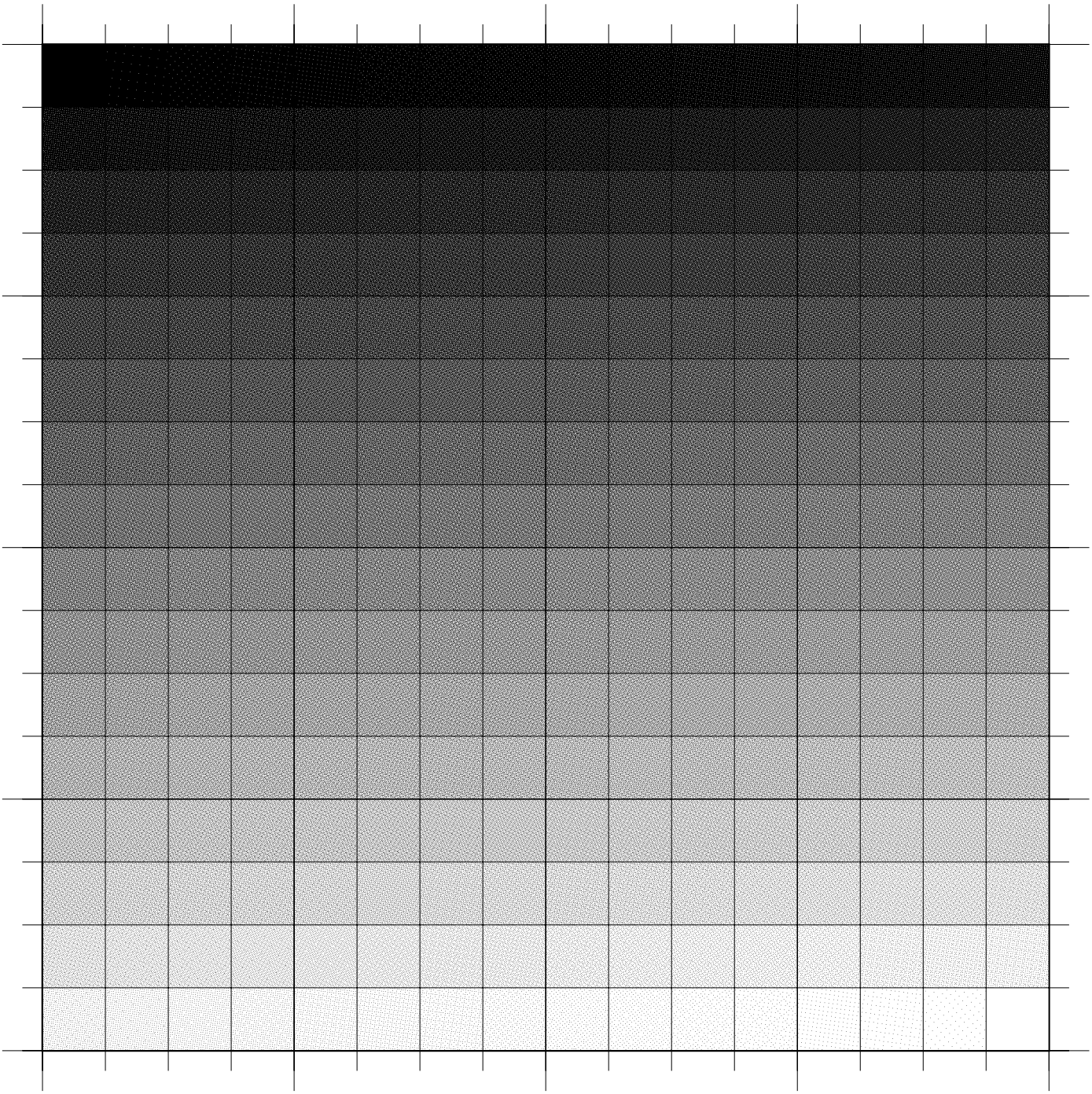

Figure 23: 256 intensity levels obtained with rotated 3x3 matrix-based Bayer-expanded dither algorithm, printed at 300 dpi on a laser printer.